Multifunctional Chiral π-Conjugated Polymer Microspheres: Production and Confinement of NLO signal, Detection of Circularly Polarized Light, and Display of Laser-Triggered NLO Emission Shifts

Radhika Vattikunta, Mari Annadhasan, Ravi Jada, Muvva Durga Prasad, Nikolai Mitetelo, Karina Zhdanova, Evgeniy Mamonov, Klaus Müllen,* Tatiana Murzina,* and Rajadurai Chandrasekar*

Two chiral π-conjugated polymers with optical nonlinearity (NLO), abbreviated as R- and S-BP, are prepared by copolymerization of R- and S-6,6'-dibromo-2,2'-diethoxy-1,1'-binaphthyl with 1,4-diethynyl-2,5-bis(octyloxy)benzene by Sonogashira coupling. The R- and S-BP copolymers self-assemble in a tetrahydrofuran/H_2O/ethanol mixture producing microspherical particles. Remarkably, the obtained polymer microspheres support excitation of whispering gallery mode resonances (500–720 nm) in one- and two-photon excited luminescence or two-photon luminescence (TPL) with a quality factor (Q) of up to ≈700. As a result of a high Q value, a single (R- or S-BP) microsphere displays a circular dichroism (CD) effect in the TPL signal. At high laser pump-power (≥10 mW), the TPL spectral features of microspheres change significantly, suggesting alterations of the polymer packing. Similar spectral variations are observed for microspheres heated thermally or with high power continuous-wave laser. Photoluminescence lifetime imaging microscopy down to the single microsphere level corroborate transformations of polymer packing from a J type to a mixture of J, H, and H-like (with disordered side chains) types. This work demonstrates the tremendous potential of tailor-made chiral polymer microspheres exhibiting multifunctional properties, such as i) light-confinement, ii) NLO-CD, and iii) laser-driven optical emission shifts, useful for many optoelectronic and photonic device applications.

1. Introduction

Recently, π-conjugated polymers (CPs)[1–3] with multifunctional properties, such as chirality, optical nonlinearity (NLO), and tunable optical emission (for example, aggregation-dependent optical emission shifts)[4] have gained vital importance. The presence of chiral groups in donor–acceptor type CP furnishes chiro-optical effects and NLO emissions, respectively. Circular dichroism (CD) is one of the chiro-optical effects which arises from the different absorption of left and right-handed circularly polarized light by enantiomeric chiral materials.[5] The envisaged applications of multifunctional CP materials include quantum information processors, phase-changing chiral systems, stereoscopic displays, chiral lasers, and chiral optical-tweezers, and chiral quantum networks, to name a few.[6–18] Hence, the synthesis and application of CPs with chirality, NLO properties, and tunable optical emission via external stimuli appear extremely promising.

The use of chiral NLO materials is limited by two critical features: i) weak NLO signals and ii) weak chiro-optical responses. Measurements of chiro-optical effects from small chiral molecules or polymers were recorded mostly in the linear optical regime.[8–10] In order to increase the strengths of NLO and chiro-optical signals, the incident light has been confined in plasmonic nanostructures, metamaterials, nanoantennae, and optical

R. Vattikunta, Dr. M. Annadhasan, R. Jada, M. D. Prasad,
Prof. R. Chandrasekar
School of Chemistry
University of Hyderabad
Prof. C. R. Rao Road, Gachibowli, Hyderabad 500046, India
E-mail: r.chandrasekar@uohyd.ac.in

The ORCID identification number(s) for the author(s) of this article can be found under https://doi.org/10.1002/adom.202000431.

N. Mitetelo, K. Zhdanova, Dr. E. Mamonov, Prof. T. Murzina
Department of Physics
Quantum Electronics Division
Moscow State University
Moscow 119991, Russia
E-mail: mur@shg.ru

Prof. K. Müllen
Max Planck Institute for Polymer Research
Ackermannweg 10, Mainz D-55218, Germany
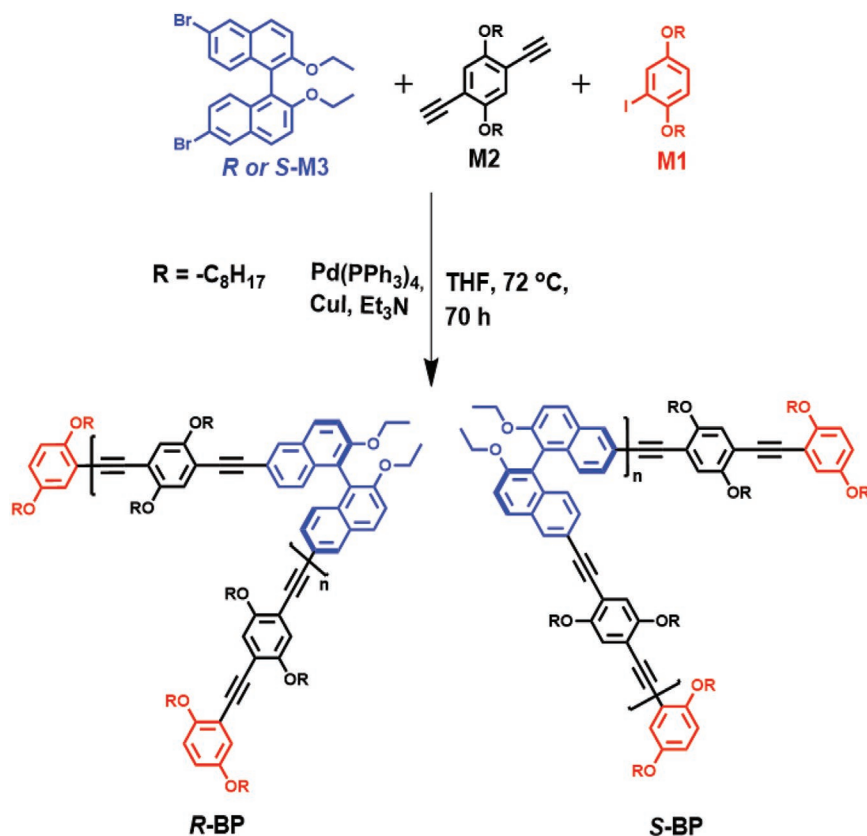E-mail: muellen@mpip-mainz.mpg.de

resonators.[11–18] In an optical resonator, the increased residence time or photon lifetime (τ_p) of the trapped incident photons is expected to increase the light-matter interaction and to amplify the signal strength.[17–21] Spherical NLO resonators obtained from solvent-assisted self-assembly of chiral polymers are particularly promising.[21] Light can be trapped via whispering gallery mode (WGM) resonance[19–25] and thus improve NLO and related CD-NLO signals. Further, polymer resonators can be obtained defect-free and with a smooth surface due to tightly packed chains. These features are essential to achieve high Q polymer optical resonators (high light storage) by minimizing scattering induced optical losses.[20]

Generally, temperature variation can cause optical emission shifts of CPs[26,27] in the solution state. The emission shift is usually attributed to H and J aggregation[28] or excimer formation,[29] and polymer backbone planarization.[30] Spano et al. have proposed a theoretical model that distinguishes H and J type aggregates based on the ratio of the first two vibronic peaks (0–0 and 0–1) of the photoluminescence (PL) spectrum.[28,31] In J type polymer aggregates, the head-to-tail arrangement of chains favors intrachain electronic coupling, and the 0–0 vibronic transition is dipole allowed. Thereby, different from the separate polymer, the $I_{0-0}^{PL}/I_{0-1}^{PL}$ (where, I_{0-0}^{PL} and I_{0-1}^{PL} are PL intensity of 0–0 and 0–1 peaks, respectively) ratio increases, the PL lifetime (τ_{PL}) decreases, and the emission bands shift to the red side of the electromagnetic spectrum.[4,28,31] In contrast, H type aggregates require a face-to-face arrangement of polymer chains, facilitating interchain electronic coupling. Here, the 0–0

transition is dipole forbidden, and the emission shifts are opposite to those seen for J type aggregates. Recently, Eder et al. have elegantly demonstrated the reversible switching of electronic coupling (H type and J type) in nanoscopic isolated CP aggregates by partially swelling and drying the aggregates embedded inside a non-photoluminescence polymer matrix.[4,28,31]

Typically, laser-based spectroscopy of organic or polymer samples employs an ultrafast pulse or continuous wave (CW) laser beam. However, above a specific pump power, the produced local heat[32,33] can induce morphological or phase changes within the polymer and, depending upon the polymer structure and molecular weight, cause a shift of the optical emission bands. Polymers that employ a similar mechanism to display diverse optical emission colors will therefore ultimately be of broader interest. However, to the best of our knowledge, a laser-triggered shift of optical emissions in CP has not found attention in the literature. We introduce here a new laser-driven technique to shift the optical emissions of chiral conjugated polymers in both linear and nonlinear optical regimes.

In this paper, we have studied chiral microresonators obtained from the self-assembly of enantiomeric π-conjugated NLO copolymers, namely, **R**- and **S**-type poly(2,2′-diethoxy-1,1′-binaphthyl-*co*-1,4-diethynyl-2,5-dioctyloxybenzene) (**R-BP** and **S-BP**). The polymers are prepared via a Sonogashira coupling (**Scheme 1**). They are composed of i) enantiomeric 1,1′-binaphthyl moieties with electron-donating ethoxy groups substituted at the 2,2′ positions; ii) moderately electron-withdrawing 1,4-diethynyl phenylene units providing aggregation-dependent

Scheme 1. Synthesis of polymers **R**- and **S-BP**.

ADVANCED
SCIENCE NEWS
www.advancedsciencenews.com

ADVANCED
OPTICAL
MATERIALS
www.advopticalmat.de

emission shifts to the polymer,[4] and iii) flexible *n*-octyloxy polymer side chains to attain solution processability. As the enantiomeric copolymers are hydrophobic, their self-assembly in tetrahydrofuran (THF) solution by adding nonsolvents (water/ethanol) produces corresponding **R**- and **S-BP** microspheres (diameter ≈3–8 μm).

Remarkably, each **R**- and **S-BP** polymer microsphere upon one- and two-photon (low-power: <2 mW) pumping functioned as optical WGM resonator (*Q*- factor up to 700) in the visible part of the electromagnetic spectrum. As a result of tight light-confinement, the CD effect in the two-photon luminescence (TPL) was detected even from a single microsphere. The TPL spectra of polymer microspheres display an intense band at ≈475 nm (0–0 transition) and a relatively broad, low-intensity band at ≈502 nm (0–1 transition). Unexpectedly, at high laser pump powers (>10 mW), a dramatic change in the emission spectra intensity with the decrease of the $I_{0-0}^{TPL}/I_{0-1}^{TPL}$ ratio occurs. Microspheres excited with CW laser (>10 mW) also demonstrated similar broadening and redshifts of the PL bands. Intuitively, these profound spectral transformations suggest changes of the polymer aggregation driven by laser-heat. Usually, ultrafast laser pulses cause more localized heating in samples compared to CW laser for the same average power.[32,33] Moreover, in both methods of laser-heating, modifying the aggregation might furnish intermediate forms next to the pure *J* and *H* type. Therefore, direct corroboration of the aggregation type from either $I_{0-0}^{PL}/I_{0-1}^{PL}$ or $I_{0-0}^{TPL}/I_{0-1}^{TPL}$ ratio is challenging. PL lifetime imaging microscopy (PLIM) of a single-microsphere confirms that the shifting of aggregation from *J*-type to a mixture of *J*, *H*, and *H*-like types. This work demonstrates that chiral CP microspheres provide access to light-confinement, TPL-CD, and laser-triggered optical emission shifts. The technique of shifting the optical emission by laser light can be extended to a broad range of CP device applications.

2. Results and Discussion

2.1. Polymer Preparation and Characterization

The *R*- and *S*-2,2′-diethoxy-1,1′-binaphthyl-*co*-1,4-diethynyl-2,5-dioctyloxy benzene copolymers end-capped with 2,5-dioctyloxy-benzene (M1) were synthesized by copolymerizing diethynyl benzene linker (M2)[34,35] and chiral monomers (*R*- and *S*-M3) via a palladium-catalyzed Sonogashira cross-coupling reaction (Scheme 1; and the Supporting Information).[36–38] The obtained polymers were purified by Soxhlet extraction with solvents like hexane to remove low molecular weight compounds/oligomers and finally with THF to collect soluble polymers. The polymers (yield 48–52%) were good soluble in common organic solvents due to the presence of flexible n-octyloxy substituents (Figure S4, Supporting Information). The THF-insoluble fractions of high molecular weight **R**- and **S-BP** polymer (yield 19–23%) were partially soluble in dimethylsulfoxide (DMSO). The remaining very high molecular weight **R**- and **S-BP** polymers (yield 16–18%) were insoluble in any solvents. In the ¹H-NMR spectra (DMSO-d_6) of **R**- and **S-BP**, the aromatic proton (see the label "*a*" in Figure S1, Supporting Information) of the end-capping unit appeared as doublet around 6.72–6.75 ppm. In the ¹³C-NMR

spectra of **R**-and **S-BP**, the acetylenic carbon peaks observed at 87.9 and 87.0 ppm (Figure S2, Supporting Information). These chemical shift values are different from those of the polymer obtained from the homocoupling of M2 (as the buta-1,3-diyne carbon peaks of the homocoupled product appear at 89.2 and 79 ppm),[39] which confirms the formation of **R**-and **S-BP** polymers. With the assumption that the majority of the polymer chain ends are end-capped, the number-average molecular weight ($\overline{M}_n$) was estimated from the ¹H-NMR spectra of **R**-and **S-BP** as ≈13 and 15 kDa (Figure S1, Supporting Information). The above results show that the molecular weight of the insoluble polymers obtained during the Soxhlet extraction is much higher than those of the DMSO soluble ones. We have used the THF soluble polymer fractions [**R-BP**: $\overline{M}_n$ ≈6.3 kDa and **S-BP**: $\overline{M}_n$ ≈7.8 kDa; see Figure S1, Supporting Information] for further studies. **R**- and **S-BPs** in THF solution ($c \approx 1.0 \times 10^{-5}$ mol L⁻¹) exhibited multiple absorption maxima at 248/278/337 nm in addition to a low energy band at ≈423 nm (**Figure** 1A). The intensity variation and redshifts shown by this ≈423 nm band
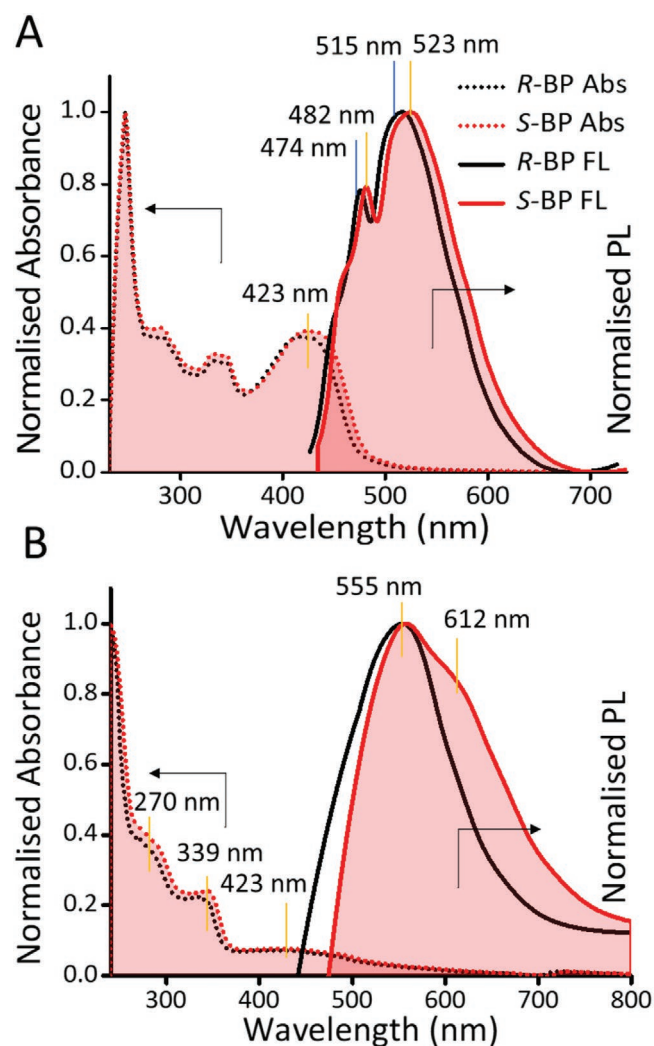

Figure 1. UV–vis absorption and PL spectra of **R**- and **S-BP** polymers in A) THF and B) thin-film state, respectively.

ADVANCED
SCIENCE NEWS
www.advancedsciencenews.com

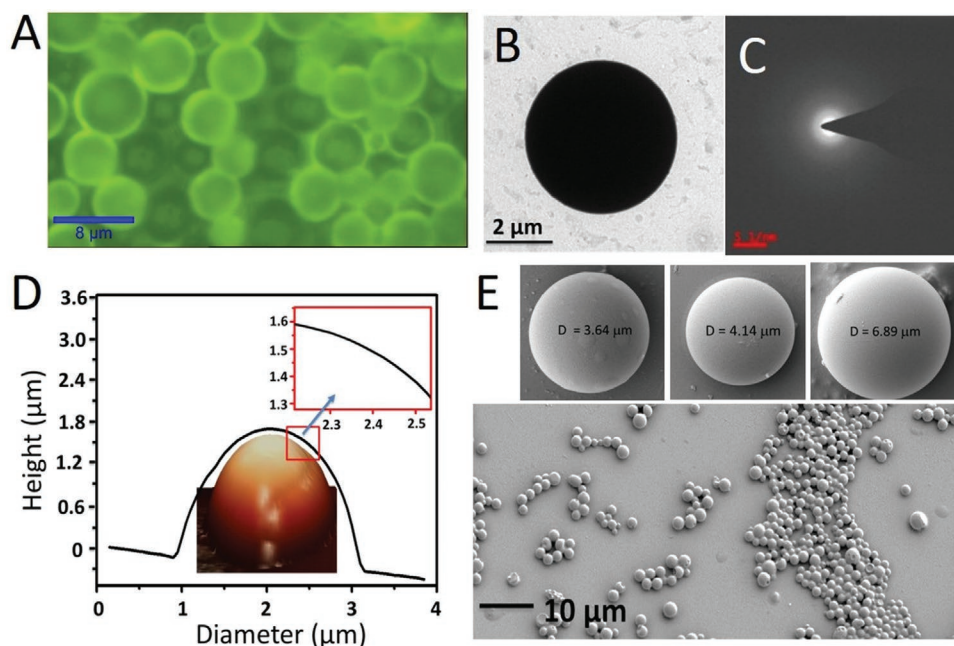ADVANCED
OPTICAL
MATERIALS
www.advopticalmat.de

Figure 2. A) Confocal optical microscope image of polymer microspheres. B,C) TEM image of a single microsphere and its SAED image, respectively. D) AFM topography image of a microsphere with its height profile (black line). The right inset shows the surface smoothness. E) FESEM images of microspheres. The top three figures present a close-up view of a single microsphere of varying diameter.

in solvents of low dielectric constants point toward its charge transfer (CT) origin (Figure S4, Supporting Information).

The solution state PL spectral features of **R-** and **S-BP** polymers are very similar (Figure 1A). Here, the redshifted (≈8 nm) PL band of **S-BP** polymer points to a better π-conjugation within the longer polymer chains. The solid-state absorption spectra of **R-** and **S-BP** polymers displayed multiple absorption maxima for both polymers (Figure 1B). In contrast to the solution, the PL bands of **R-** and **S-BP** polymers in the solid-state appeared broad with maxima at 555 nm together with a shoulder at 612 nm. The estimated NLO absorption coefficients (β) of **R-** and **S-BP** polymers (0.124×10^{-11} and 0.155×10^{-11} cm W^{-1}, respectively) using an open aperture Z-scan technique confirm their NLO properties (Figure S5C, Supporting Information).

Microparticles of **R-** and **S-BP** polymers were prepared on a cover-slip using a self-assembly technique (see Section S2.2, Supporting Information). Here, the formation of microspheres from hydrophobic polymers was driven by water (poor solvent for the polymers).[21] The examination of the sample under confocal optical microscopy revealed spherical microparticles (Figure 3A). The obtained result was supported by field-emission scanning electron microscope (FESEM) analysis which showed a relatively narrow size-distribution with diameters of ≈3–8 μm (**Figure 2**E). Transmission electron microscopy (TEM) studies displayed dark contrast for the microspheres, which indicates a dense packing of the polymer chains (Figure 2B). Selected-area electron diffraction (SAED) patterns of a single microsphere showed no identifiable diffraction spots establishing their amorphous nature (Figure 2C). Atomic force microscopy (AFM) revealed that the surface smoothness of the microspheres was below the detectable limit (<0.01 μm). This finding is essential for minimizing light scattering loss and increasing the Q-factor (Figure 2D). To understand the

influence of polymer conformation and packing in self-assembled microspheres, the evolution of absorption and CD spectroscopic signatures of THF solution of **R-** and **S-BP** polymers with different volume fractions ($f_{water:EtOH(7:1)} = 0$–70%) of the antisolvent mixture were investigated, which are given in Figures S5A,B and S6 (Supporting Information).[40]

2.2. Light-Trapping Studies of R- and S-BP Microspheres

To probe the light-trapping ability of **R-** and **S-BP** microspheres, we carried out single-microsphere PL experiments with confocal microscopy. Electronic excitation of an edge of a single microsphere with a CW laser (488 nm, Ar$^+$; power: 5 mW) displayed a ring-shaped green emission along the microsphere boundary (**Figure 3**A, insets). The corresponding PL spectrum (500–750 nm region) exhibited multiple pairs of sharp peaks (Figure 3A), indicating the formation of a WGM cavity.[20] These pairs of peaks correspond to transverse electric and transverse magnetic modes. The free spectral range (FSR) or the spacing between two adjacent peaks of three representative **S-BP** microspheres of different sizes are presented in Figure 3A. For a typical WGM resonator, the FSR value is inversely related to diameter as per the following equation, FSR $= \lambda^2/\pi D n_{eff}$, where D is the diameter, n_{eff} is the effective refractive index, and λ is the peak wavelength. Satisfying the above equation, microspheres of three different diameters, $D \approx 7.6$, 6.2, and 3.9 μm exhibited FSR values of 10.1, 14.1, and 20.4 nm. A nearly linear relationship revealed by the FSR versus 1/D plot (Figure 3B) confirms the size-dependency of the polymer WGM microresonators. Further, the number of optical modes decreased from 38 to 18 upon reducing the resonator size from 7.6 to 3.9 μm. These results unambiguously confirm that the
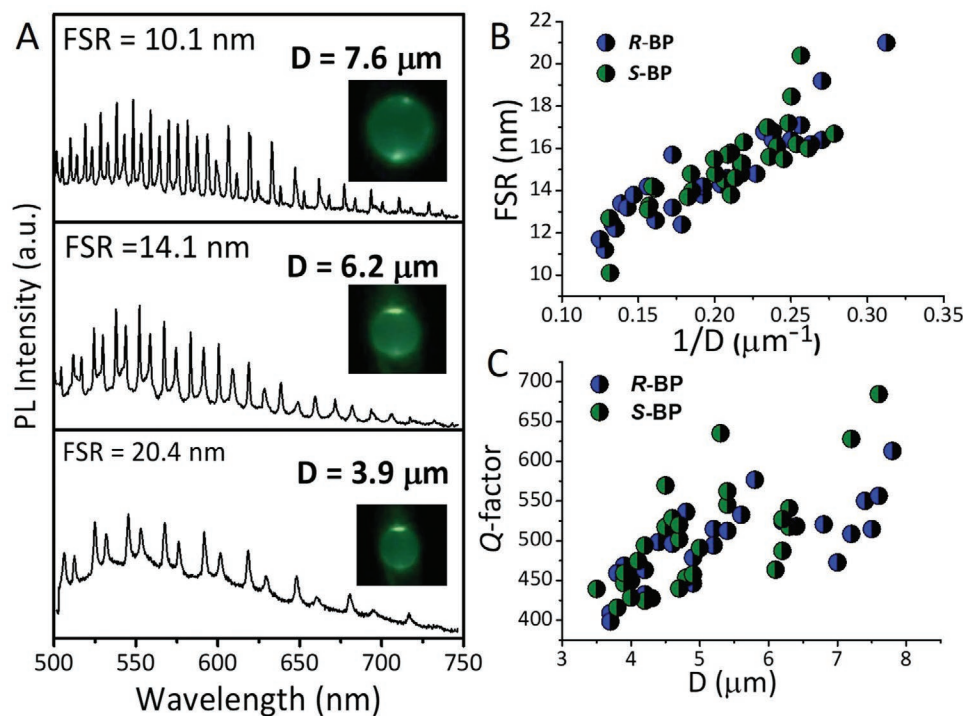
ADVANCED
SCIENCE NEWS
www.advancedsciencenews.com

ADVANCED
OPTICAL
MATERIALS
www.advopticalmat.de

Figure 3. A) Particle size-dependent single-particle PL spectra of microspheres of **S-BP** exciting WGM resonances. The insets display the PL images of microresonators excited with CW laser (488 nm; Ar^{+}). B) A plot of FSR versus 1/D for **R-** and **S-BP** microresonators. The line shows the linear fits. C) A plot of Q-factor versus particle D for **R-** and **S-BP** microresonators.

microspherical particles function as WGM resonators.[19] Similarly, **R-BP** microspheres gave particle size-dependent WGM resonances (Figure 3B; and Figure S6, Supporting Information). The Q-factor of an optical resonator is equal to $\lambda/\Delta\lambda$; where $\Delta\lambda$ is the line width of a peak at full-width at half-maximum. Both **S-** and **R-BP** microspheres provided Q-factors in the range of ≈400–≈700 (Figure 3C). The increase of the Q-factor with increasing microsphere diameter due to the exponential reduction of bending radiation loss with resonator size.

2.3. TPL and CD-NLO Effect from Polymer Optical Microresonators

The NLO properties of **R-** and **S-BP** microresonators were explored by exciting a single microresonator with a Ti: Sapphire femtosecond (fs) pulse laser (λ_{ex} = 740 nm, pulse width 60 fs, repetition rate 80 MHz). At low power (4 mW), both **R-** and **S-BP** microresonators (D≈13 and 9 μm, respectively) revealed remarkable WGM signatures in their TPL spectra (**Figure 4**A,B). The TPL spectra of **R-** and **S-BP** microresonators comprised a high-intensity 466 nm peak (0–0 transition) and a relatively broad low-intensity ≈502 nm peak (0–1 transition). Due to strong light confinement, even a single microresonator (**R-** or **S-BP**) is expected to exhibit a CD effect in the TPL signal. The schematic description of the CD(TPL) experiment is presented in Figure 4C. The TPL intensity of a single microresonator when excited with left-circularly polarization (LCP) and right-circularly polarization (RCP) fundamental light of different wavelengths showed that the TPL intensity variation is prominent

at the region of maximum two-photon absorption (TPA), i.e., at 750 nm (Figure S7, Supporting Information). Further, **R-** and **S-BP** microresonators demonstrated a noticeable TPL intensity difference upon excitation with light of matching handedness. For CD(TPL) the following coefficient was used[20]

$$CD\left(TPL\right) = \frac{I\left(RCP\right) - I\left(LCP\right)}{I\left(RCP\right) + I\left(LCP\right)} \tag{1}$$

where LCP and RCP stand for left and right circularly polarized fundamental lights, respectively. I(RCP) and I(LCP) are the TPL intensity of the RCP, and LCP, respectively. The calculated CD(TPL) values over the whole spectral range (880–750 nm) for both **R-** and **S-BP** microresonators were nearly constant in the range of ≈6% (with opposite signs) without any apparent spectral dependence (Figure 4D; and Figure S7, Supporting Information). As mentioned earlier, both CD and TPL signals are usually weak.[3,8,20] However, the manifestation of a CD effect in the TPL signal from a single microresonator (**R-** or **S-BP**) points at the increased light-polymer interaction owing to optical field confinement.

2.4. Polymer Chain Packing-Dependent Electronic Coupling

To probe the pump-power dependencies of the TPL spectra, **R-** and **S-BP** microresonators were excited at different fs laser pump powers. Unexpectedly, at high pump power, the profile of the TPL spectra changed drastically. The 0–1 peak was selectively amplified relative to the 0–0 peak (Figure 6A,B). The change in
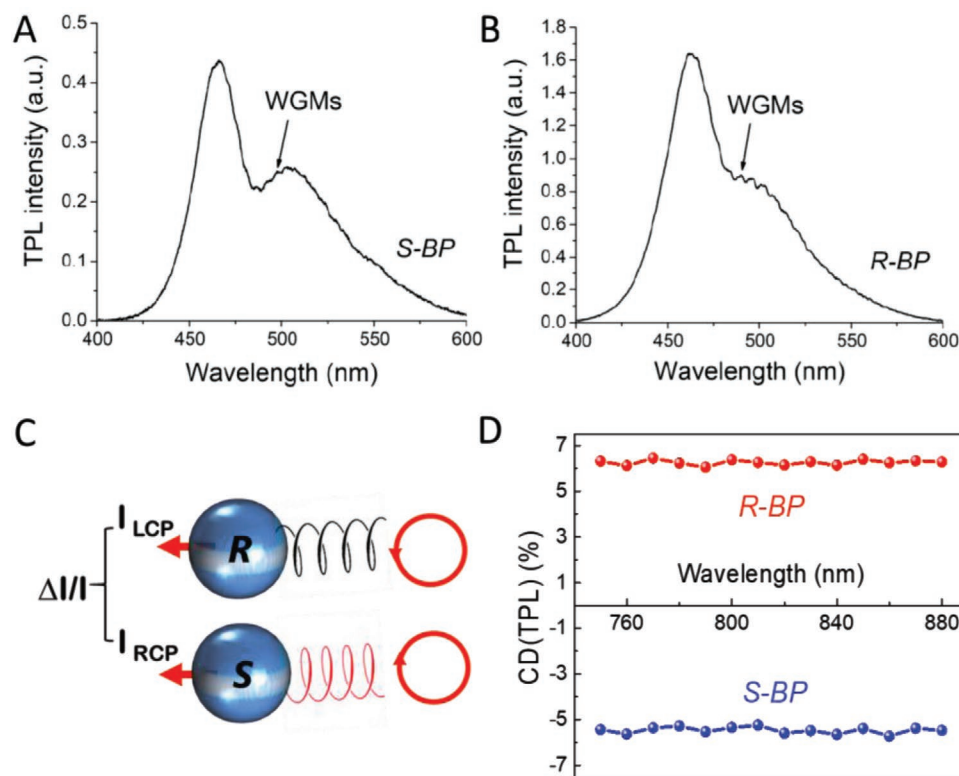
Figure 4. A,B) TPL spectra revealing WGM excitation for single **R-** and **S-BP** microresonators. C) Schematic illustration of the excitation of **R-** and **S-BP** microspheres by left- and right-polarized light. D) TPL-CD signal of **R-** and **S-BP** microspheres as a function of pump wavelength.

the ratio of $I_{0-0}^{TPL}/I_{0-1}^{TPL}$ at high pump power indicates a dramatic change of the polymer packing within the microresonators. Generally, ultrafast laser pulses cause more localized heating (a lower heat-affected region) in samples compared to CW laser.[32,33] Further, the short-pulse laser raises the sample temperature more than the CW laser of the same average power. The temperature-dependent PL spectra ($\lambda_{ex} = 405$ nm CW laser; 5 mW) of **R-** and **S-BP** microresonators also led to an increased intensity of the 0–3 peak accompanied by a redshift with rising temperature (**Figure 5**C,D; and Figure S8, Supporting Information), confirming heat-induced changes of the polymer packing.[32] However, the PL spectra of thermally heated samples could not be entirely matched with TPL spectra as the latter samples were heated by fs pulse laser and arise from TPA processes.

The applicability of Spano's model is straightforward for polymer systems with a homogeneous distribution of polymer chain packing (either H or J), but not when J and H aggregates exist side by side. It is nevertheless expected that the microspheres with mixed polymer chain packing would reveal aggregation-type dependent PL lifetimes (τ_{PL}). Thus, we probed τ_{PL} of a single microsphere by the PLIM technique. For a fair comparison of results, we used the same microsphere before and after irradiation with high laser power (CW 405 nm) or heating thermally (**Figure 6**). The PLIM image of **R-** and **S-BP** microspheres before treating them with high laser power (15 mW) exhibited a single exponential PL decay with uniformly distributed average τ_{PL} values of 0.54–0.61 ns (Figure 6A,B). However, the same microspheres after laser treatment revealed different τ_{PL} values, a shorter radiation time at the center of the microsphere (pump

area), moderate radiation time around the pump area (≈5 ns), and a much longer radiation time (up to≈10 ns) from the periphery (Figure 6C,D). Here, the regions with higher and lower τ_{PL} values point to H (interchain electronic coupling) and J (intrachain electronic coupling) type polymer chain packing, respectively.[28,30,41] The regions with intermediate τ_{PL} possibly arise from a polymer chain packing closer to the H type[42] with disordered octyl side chains. The increase of τ_{PL} from the center of the microsphere to its periphery validates the gradual transformation of polymer chain packing type due to laser-induced heating. The τ_{PL} also indicates that polymer chains are tightly packed at the periphery of the microspheres compared to its center.

The $I_{0-0}^{TPL}/I_{0-1}^{TPL}$ ratios of **R-** and **S-BP** polymer microspheres excited with a fs laser at low pump power (<1 mW) were in the range of 1.4–1.7 (Figure 4A,B), which is close to J type polymer packing (with a homogeneous distribution of τ_{PL}). Nevertheless, it may not be the predominant one; for example, in the case of trans-polydiacetylene polymer chains, the ratio goes up to several hundreds[26,27] due to an effective long-range J coupling. However, at high fs laser power (>10 mW) these microspheres show a decrease in the $I_{0-0}^{TPL}/I_{0-1}^{TPL}$ ratio (Figure 5E) due to a substantial reduction of the 0–0 peak intensity, which validates H-type coupling detected in the peripheral regions by the PLIM measurements. The **R-** and **S-BP** polymer microspheres heated either with CW laser (>10 mW) or thermally (>80 °C) showed a decreasing of $I_{0-0}^{TPL}/I_{0-1}^{TPL}$ ratio (Figure 6F,G). Nevertheless, in both cases, the 0–0 and 0–1 peak intensities reduced considerably (Figures 5C,D and 6C,F) due to mixed polymer chain packing. Further, the manifestation of slightly broadened and redshifted PL bands
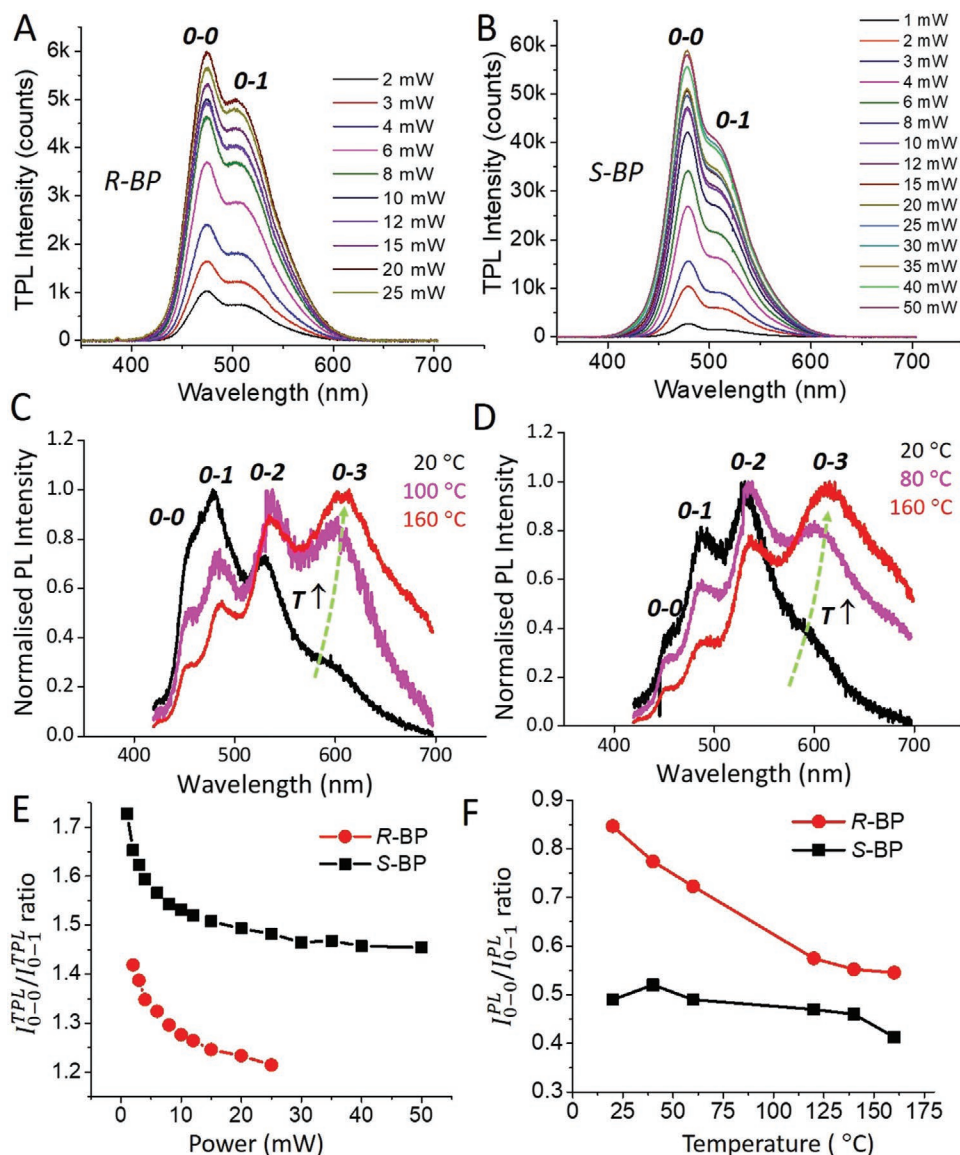
**ADVANCED
SCIENCE NEWS**

www.advancedsciencenews.com

**ADVANCED
OPTICAL
MATERIALS**

www.advopticalmat.de

Figure 5. A,B) TPL spectra of *R*- and *S*-BP microresonators as a function of pump power. C,D) Temperature-dependent PL spectra of *R*- and *S*-BP microresonators. The ratio 0–0/0–1 optical emission peak intensities as a function of E) fs laser power and F) thermal heating for *R*- and *S*-BP microspheres.

(0–3 vibronic peak) with high intensity (Figures 5C,D and 6C,F) arises due to intrachain planarization of the aromatic backbone in the center of the microsphere (more *J* character),[4,41] and excimer-like transition[31] from the peripheral regions of the microsphere. One of the unprecedented applications of the above experiments is that these laser-triggered aggregation changes can be effectively used to control the electronic coupling in conjugated polymers.

3. Conclusion

We have synthesized two novel chiral-NLO-CPs, abbreviated as *R*- and *S*-BP via Sonogashira cross-coupling reaction with $\overline{M_n}$ = 13 and 15 kDa, respectively. The obtained polymers self-assemble into microspheres (diameter ≈3–8 µm) in THF/ethanol/water mixtures. Individual microspheres displayed PL

spectra with WGMs having a *Q*-factor of up to 700. The high *Q*-factor confirms the potential of *R*- and *S*-BP microspheres for nanophotonic devices. Due to the donor–acceptor interactions, these *R*- and *S*-BP microresonators, upon two-photon excitation (at low pump power), exhibited TPL together with WGMs. A noteworthy feature of the chiral *R*- and *S*-BP microspheres is that upon excitation with CPL of different handedness, they revealed a much sought after CD effect in the TPL signal with values ≈6%. The observation of a (generally weak) CD effect in the TPL of a single (*R*- or *S*-BP) microresonator confirms amplified light-polymer interaction due to its high *Q*-factor.

At high two-photon pump power (>10 mW), due to laser-triggered heating, *R*- and *S*-BP microspheres exhibited significant alteration of the TPL spectral feature (decrease of the ratio of 0–0/0–1 bands). The hypothesis that the spectral transformation is due to ultrafast laser-triggered heating was
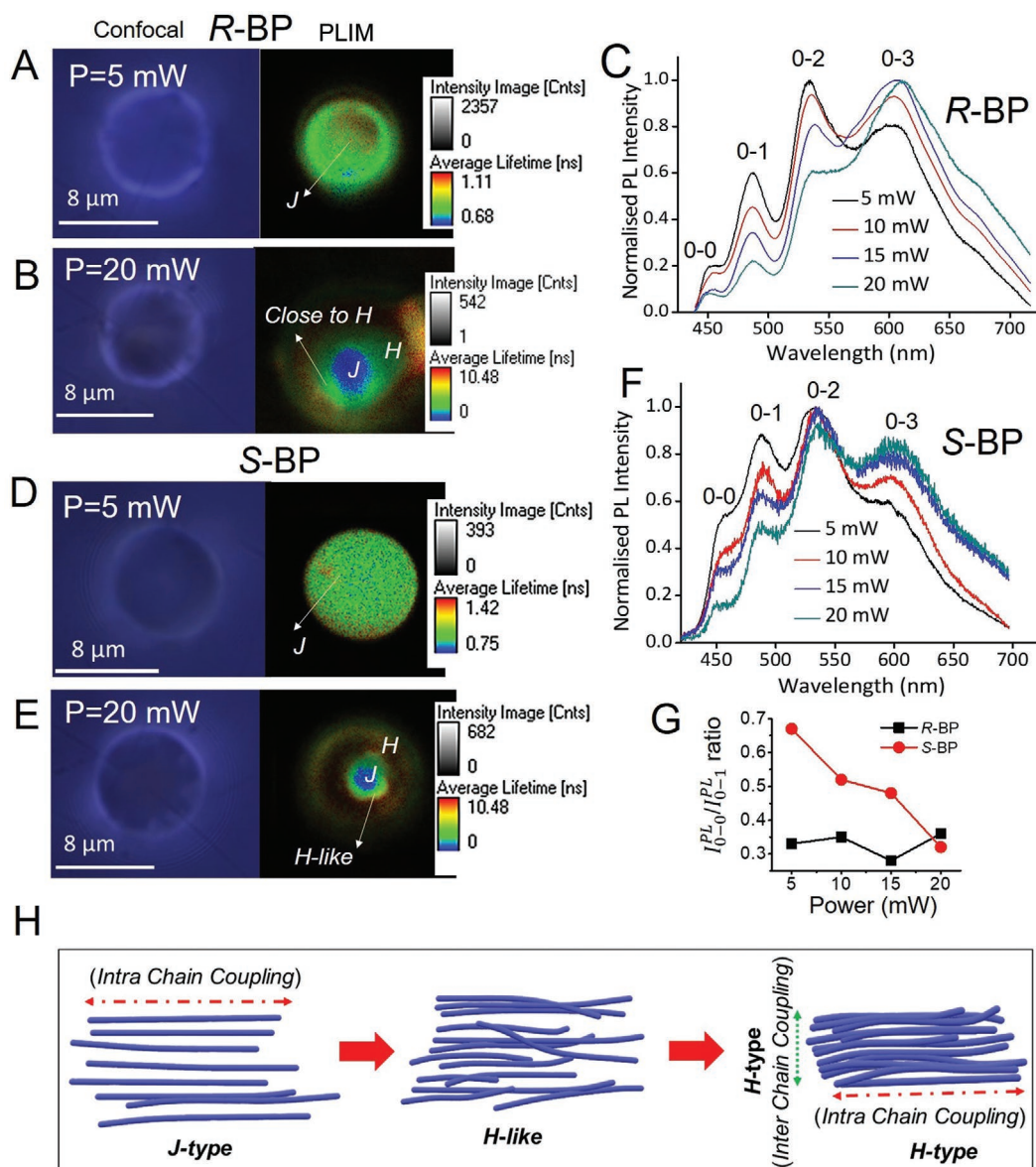
**ADVANCED
SCIENCE NEWS**

www.advancedsciencenews.com

**ADVANCED
OPTICAL
MATERIALS**

www.advopticalmat.de

Figure 6. Confocal microscopy (left) and the corresponding PLIM (right) images of *R*- and *S*-BP microspheres: A,B) before and D,E) after laser-induced heating. C,F) PL spectra of *R*- and *S*-BP microspheres (used in PLIM experiments) at different CW laser (450 nm) pump powers. G) The ratio 0–0/0–1 optical emission peak intensities as a function of CW laser power for *R*- and *S*-BP microspheres. H) Schematic illustrating the mechanisms of *H*, *J*, and *H*-like coupling in *R*- and *S*-BP polymers.

confirmed by heating the microspheres thermally. Additionally, pump-power-dependent PL spectra showed line broadening and slight redshifts at high pump powers. As the observed spectral alteration is a direct indicator of the changes in inter- and intrapolymer chain electronic coupling, PLIM experiments were carried out for microspheres. The obtained τ_{PL} image of *R*- and *S*-BP microspheres confirmed the shifting of *J* type polymer packing to a mixed type (*H*, *J*, and close to *H*-like) after exposure to the high-power laser beam. Our proof-of-concept experiment demonstrated that laser-driven optical emission shifts in CPs can be realized by transforming polymer packing from one type to another (*J* to *H* and vice versa). Further, smart polymer microspheres with multifunctional properties (light-trapping ability, CD-NLO, and

laser-driven optical emission shifts) are promising candidates for their utility in cutting-edge areas of nanophotonics, such as chiral light emitters, phase-changing chiral optical components, stereoscopic displays, and chiral lasers.

4. Experimental Section

Synthesis of 2-iodo-1,4-dioctyloxybenzene (M1): 1,4-dioctyloxybenzene (1 g, 2.98 mmol, 1 eq.) was taken in a round-bottomed flask containing acetic acid (10 mL) and H_2SO_4 (0.1 mL). To this reaction mixture, a solution containing KIO_3 (127 mg, 0.6 mmol, 0.2 eq.), I_2 (378 mg, 0.2 eq.), two drops of conc. H_2SO_4 and H_2O (1 mL) were added by dropwise. The reaction was heated to reflux for 5 h. The progress of the reaction was monitored by thin-layer chromatography (TLC) to check the

**ADVANCED
SCIENCE NEWS**

www.advancedsciencenews.com

**ADVANCED
OPTICAL
MATERIALS**

www.advopticalmat.de

formation of the monoiodinated product. When a maximum amount of monoiodinated product was formed, the reaction was stopped by adding an aqueous $Na_2S_2O_3$ solution to quench any excess I_2. The precipitate formed was collected by filtration and extracted with $CHCl_3$, dried over Na_2SO_4 and evaporated in vacuo. The obtained crude compound was purified by column chromatography on silica gel with n-hexane/EtOAc (95:5 v/v) as eluents to get M1 (0.23 g, 82%) ^1H NMR (400 MHz, $CDCl_3$, δ): 6.83 (dd, 1H), 6.72 (d, 1H) 7.34 (d, 1H), 3.93 (t, 2H), 3.87 (t, 2H), 1.84–0.90 (m, 24H), 0.88 (t, 6H). ^{13}C-NMR (100 MHz, $CDCl_3$) δ (ppm): 153.69, 152.07, 125.32, 115.36, 113.09, 87.00, 70.24, 68.89, 31.99, 29.66, 29.42, 29.38, 26.19, 26.09, 22.76, and 14.19.

Synthesis of 1, 4-diethynyl-2,5-bis(octyloxy)benzene (M2): A mixture of 2,5-diiodo-1, 4-dioctyloxybenzene (5 g, 8.5 mmol, 1 eq.), $Pd(PPh_3)_2Cl_2$ (300 mg, 0.427 mmol, 0.05 eq.), and CuI (150 mg, 0.789 mmol, 0.1 eq.), were taken in a clean and dry two neck round-bottomed flask. The flask was subjected to a freeze-pump-thaw cycle three times. To this mixture, dry Et_3N (60 mL) was added under N_2 atmosphere. Later, trimethylsilylacetylene (3.5 mL, 25.5 mmol, 3 eq.) was added dropwise to the reaction mixture. The reaction was continued with stirring for 12 h at 70 °C. After cooling, the solvent was removed in vacuo and the residue was purified by chromatography on a short plug of silica gel with n-hexane/ethyl acetate (95:5 v/v) as eluent to afford golden colored oil (4.7 g, 83%) that solidified slowly upon storing at rt. Subsequently, the as-obtained product was dissolved in THF (35 mL) and methanol (50 mL). Later, an aqueous NaOH (2.5 N, 7.5 mL) was added to the reaction mixture. The deproduction reaction was continued with stirring at rt for 5 h. The solvent was concentrated under reduced pressure. To the residue was added a mixture of H_2O (20 mL) and CH_2Cl_2 (20 mL) to afford a two-phase solution. The organic layer was separated and concentrated under reduced pressure to get the target compound M2 as yellow solid (3.4 g, 97%). ^1H NMR ($CDCl_3$, 400 MHz, δ): 6.94 (s, 2H, Ph-H), 3.98 (t, 4H, O—CH_2), 3.33 (s, 2H, $\equiv$C—H), 1.78 (m, 4H), 1.54–1.28 (m, 20H), 0.9 (s, 6H, CH_3). ^{13}C-NMR ($CDCl_3$, 100 MHz, 298 K): δ(ppm) = 151.3, 117.4, 109.2, 81.9, 78.7, 68.1, 31.9, 29.7, 29.3, 25.9, 22.6, and 14.1.

Synthesis of R- and S-6, 6'-dibromo-2, 2'-diethoxy-1, 1'-binaphthyl (M3): A suspension of R- and S-1,1'-binaphthol (2.0 g, 7 mmol) in acetonitrile (20 mL) was stirred under N_2 atmosphere, later K_2CO_3 (3.8 g, 28 mmol) and C_2H_5Br (1.5 mL, 21 mmol) were added to it and the mixture was heated to reflux at 85 °C for 24 h. The solvent was removed in vacuo, and the mixture was diluted with CH_2Cl_2 (30 mL). The organic layer was further washed with H_2O and brine and dried over anhydrous Na_2SO_4. After removal of the solvent, the residue was purified by column chromatography (silica gel, hexane-EtOAc, 95:5) to give 2,2'-diethoxy-1,1'-binaphthalene as a viscous liquid. Yield (1.86 g, 78%). ^1H NMR (400 MHz, $CDCl_3$, δ): 7.93 (d, 2 H), 7.85 (d, 2 H), 7.42 (d, 2 H), 7.42 (d, 2 H), 7.30 (dd, 2H), 7.20 (dd, 2H), 7.13 (br d, 2 H), 4.04 (m, 4 H), 1.05 (t, 6H). ^{13}C NMR (100 MHz, $CDCl_3$, δ): 154.22, 134.08, 129.15, 128.97, 127.68, 125.93, 125.40, 123.31, 120.58, 115.77, 65.10, 14.88. 2,2'-diethoxy-1,1'-binaphthalene (2 g, 5.8 mmol) was dissolved in CH_2Cl_2 (50 mL) and cooled to 0 °C. Br_2 was added to it in increments, starting with 1.8 eq. until the reaction went to completion. The reaction mixture was then extracted with 10% NaHSO$_3$ and brine. After drying over Na_2SO_4 and filtering, the solvent was removed to yield the product R- and S-6,6'-dibromo-2,2'-diethoxy-1,1'-binaphthalene as an oil (2.14 g, 74%). ^1H NMR (400 MHz, $CDCl_3$, δ): 8.00 (d, 2H), 7.84 (d, 2H), 7.42 (d, 2H), 7.26 (dd, 2H), 6.95 (d, 2H), 4.03 (m, 4H), 1.06 (t, 6H), ^{13}C NMR (100 MHz, $CDCl_3$, δ): 154.42, 132.41, 130.11, 129.68, 129.34, 128.32, 126.98, 119.93, 117.16, 116.35, 64.96, and 14.89.

Syntheses of R- and S-BP Polymers: R- or S-M3 (178 mg, 0.35 mmol), M2 (136 mg, 0.356 mmol), Pd(PPh$_3$)$_4$ (41 mg, 0.03 mmol), and copper(I) iodide (7 mg, 0.03 mmol) were added to a mixture of solvents of THF (8 mL) and Et_3N (4 mL) under N_2 atmosphere. The mixture was stirred at 70 °C under N_2. The polymer end-capping group, namely M1 (32 mg, 0.03 mmol, 0.2 eq.) was added to the reaction 15 min after starting the polymerization. After 72 h, the mixture was cooled to rt and the solvent was evaporated. Then the residue was washed with CH_3OH to remove any small molecular impurities. The Sonogashira coupling reaction product was dried under vacuum overnight to obtain R- and S-BP with 0.071 g and 0.192 g, respectively. The obtained polymer was subjected to

Soxhlet extraction (acetonitrile, $CHCl_3$ and lastly with THF) to discard low molecular weight fractions and isolate soluble high molecular weight polymer. **S-BP**: ^1H NMR (400 MHz, $CDCl_3$, δ): 8.02 (s, 20H), 7.82–7.85 (d, 22H), 7.72 (s, 9H), 7.64–7.69 (m, 52H), 7.53–7.56 (m, 30H), 7.44–7.48 (m, 58H), 7.40–7.42 (m, 26H), 7.33–7.35 (m, 3H), 7.31–7.32 (m, 6H), 6.90–6.95 (m, 39H), 6.81–6.83 (d, 2H), 6.70–6.73 (d, 2H), 4.02–4.04 (m, 70H), 3.95–3.97 (m, 32H), 3.91–3.92 (m, 8H), 3.85–3.88 (m, 10H), 1.04–1.09 (m, 113H), 0.86–0.88 (m, 174H). **R-BP**: ^1H NMR (400 MHz, $CDCl_3$, δ): 8.02 (s, 14H), 7.83–7.85 (d, 14H), 7.72 (s, 3H), 7.65–7.68 (m, 23H), 7.53–7.55 (m, 12H), 7.45–7.48 (m, 25H), 7.41–7.42 (m, 16H), 7.31–7.33 (m, 3H), 7.24–7.2 6 (m, 3H), 6.94–6.95 (m, 18H), 6.81–6.83 (d, 2H), 6.71–6.73 (d, 2H), 4.04–4.06 (m, 36H), 3.95–3.97 (m, 6H), 3.91–3.92 (m, 6H), 3.85–3.88 (m, 6H), 1.04–1.07 (m, 77H), 0.86–0.88 (m, 151 H). $\overline{M_n}$ [by ^1H-NMR] $\approx$15 and 13 kDa for **R**- and **S-BP** polymers, respectively. ^{13}C NMR (100 MHz, $CDCl_3$, δ): 154.54, 132.52, 132.22, 132.12, 132.04, 131.90, 130.34, 130.23, 129.85, 129.77, 129.65, 129.45, 129.29, 128.75, 128.52, 128.42, 127.54, 127.08, 125.37, 120.07, 117.27, 116.48, 115.45, 113.16, 70.22, 69.78, 68.87, 65.07, 37.08, 32.73, 31.90, 31.78, 30.31, 30.01, 29.67, 29.63, 29.33, 29.30, 29.26, 29.21, 29.05, 27.06, 26.07, 26.04, and 25.97.

For **S-BP**, the relative signal intensities of binol proton (marked as "d") to protons of 1,4-dioctyloxybenzene of end group (marked as "a") was 34:2. This ratio suggested degrees of polymerization ($\overline{X_n}$) of 17, corresponding to $\overline{M_n}$ of about 13 kDa. A similar analysis revealed $\overline{X_n}$ value of about 19.5 for **R-BP** with $\overline{M_n}$ of $\approx$15 kDa.

Preparation of R- and S-BP Polymer Microspheres: Hydrophobic **R**- and **S-BP** polymers were converted into microspheres via solvent-assisted self-assembly. In brief, in a clean vial 1 mg of either **R**- or **S-BP** was dissolved in 1 mL of THF, and the obtained solution was transferred slowly along the walls of a vial containing a mixture of 2 mL of H_2O/EtOH (7:1). The resulting turbid solution was kept undisturbed for 6 h, followed by drop-casting 2–3 drops of it on a coverslip. The solvents were evaporated slowly under ambient conditions to obtain microspheres covering a large surface area of the coverslip.

Characterization: ^1H and ^{13}C NMR spectroscopy studies were recorded on a Bruker DPX 500 spectrometer with solvent proton as an internal standard ($CDCl_3$-d_1 = 7.26 ppm). UV–visible absorption spectra were recorded on a SHIMADZU-UV-3600 UV–VIS–NIR Spectrophotometer. High-resolution mass analysis was performed on a Bruker ESI-TOF mass spectrometer. Size and morphology of the microspheres were examined by using a Zeiss FESEM operating at 3 kV. IR spectra were recorded on Nicolet 5700 FTIR or JASCO FT/IR 5300. For TLC, silica gel plates Merck 60 F254 were used and compounds were visualized by irradiation with UV light.

Atomic Force Microscopy: AFM studies were carried out on NT-MDT Model Solver Pro M microscope using a class 2R laser of 650 nm wavelength having a maximum output of 1 mW. All calculations and image processing were carried out by using NOVA 1.0.26.1443 software provided by the manufacturer. The images were recorded in a semicontact mode using a super sharp silicon cantilever (NSG 10-DLC) with a diamond-like carbon tip (NT-MDT, Moscow). The dimension of the tip is as follows: cantilever length 5100 (65) mm, cantilever width 35 (65) mm, and cantilever thickness 5 1.7–2.3 mm, resonance frequency 5 190–325 kHz, force constant 5 5.5–22.5 N m^{-1}, reflective side 5 Au, tip height 5 10–20 nm, and DLC tip curvature radius 1–3 nm.

Confocal Microspectroscopy: The single-particle microspectroscopy experiment of microrod was carried out on a transmission mode set-up of the Wi-Tec alpha 300 AR laser confocal optical microscope equipped with a Peltier-cooled charge-coupled device (CCD) detector. 300 grooves mm^{-1} grating BLZ = 750 nm was used, with the accumulation time of 10 s and integration time of 1.0 s. To acquire a single spectrum ten accumulations were performed. A diode 405 nm laser was employed as an excitation source. A 150× objective was used for the selective excitation of a single microsphere. Laser power was estimated using THOR Labs power meter (see Figure S12, Supporting Information).

NLO Microscopy: The experimental setup was based on femtosecond Ti:Sapphire laser with the wavelength-tunable in the range 740–880 nm, pulse frequency 80 MHz, pulse duration 60 fs. During nonlinear optical studies the fundamental beam was focused on the sample by Mitutoyo 100x objective with NA = 0.7, so that the focused beam

diameter at the wavelength of 740 nm was about 1 µm. This is much smaller as compared to the typical microsphere diameter of 3–8 µm. The nonlinear optical signal (two-photon fluorescence) was collected by the identical Mitutoyo 100x objective in "transmission" geometry (Figure 4 and 5) and collected by a photomultiplier tube (PMT) Hamamatsu R4220P with an appropriate (see below) set of filters that cut-off the fundamental beam, so the full intensity of different spectral components of the nonlinear optical signal were measured. In some of the experiments, a home-made spectrometer with the spectral resolution of < 1 nm, based on Hamamatsu S10141-1107S-01 CCD image sensor, was used. For the investigations of the NLO-CD effect, LCP or RCP of the laser beam was made by a zero-order quarter-wavelength plate aligned at the proper angle. The laser beam was focused approximately to the center of the microsphere, in order to increase the measured TPF signal. After passing through the microsphere, the TPF radiation was spectrally selected by BG39 filter, so the intense fundamental beam was cut-off, and detected by PMT (see Figure S13, Supporting Information).

PLIM: PL decays and PL lifetime images were recorded on a time-resolved (Micro-Time 200, Pico Quant) confocal PLIM setup, which was equipped with an inverted microscope (Olympus IX 71). Measurements were performed at room temperature, on a microparticles deposited cover-slip. The samples were excited by a 405 nm ps diode pulse laser (power ≈5 µw) with a stable repetition rate of 20 MHz (FWHM: 176 ps) through a water immersion objective (Olympus UPlans Apo; 60 ×; NA 1.2). Signal from the samples was collected by the same objective and passed through the dichroic mirror, filtered by using a 430 nm long-pass filter to cut off any exciting light. The signal was then focused onto a 50 µm diameter pinhole to remove the out-of-focus signal, recollimated, and directed onto a (50/50) beam splitter prior to entering two single-photon avalanche photodiodes. The data acquisition was carried out with a SymPhoTime software-controlled PicoHarp 300 time-correlated single-photon counting module in a time-tagged time-resolved mode. The overall resolution of the setup was 4 ps.

Supporting Information

Acknowledgements

Conflict of Interest

The authors declare no conflict of interest.

Keywords

[1] X. Guo, M. Baumgarten, K. Müllen, *Prog. Polym. Sci.* **2013**, *38*, 1832.
[2] S. R. Marder, J. W. Perry, *Science* **1994**, *263*, 1706.
[3] M. J. Cho, D. H. Choi, P. A. Sullivan, A. J. P. Akelaitis, L. R. Dalton, *Prog. Polym. Sci.* **2008**, *33*, 1013.
[4] T. Eder, T. Stang, M. Gmelch, K. Remmerssen, D. Laux, S. Höger, J. M. Lupton, J. Vogelsang, *Nat. Commun.* **2017**, *8*, 1641.
[5] F. Peer, F. Hache, *Chirality* **2005**, *17*, 421.
[6] G. D. Fasman, *Circular Dichroism and Conformational Analysis of Biomolecules*, Plenum Press, New York **1996**.
[7] P. Lodahl, S. Mahmoodian, S. Stobbe, A. Rauschenbeutel, P. Schneeweiss, J. Volz, H. Pichler, P. Zoller, *Nature* **2017**, *541*, 473.
[8] N. Berova, K. Nakanishi, R. W. Woody, *Circular Dichroism: Principles and Applications*, Wiley-VCH, Weinheim **2000**, p. 337.
[9] A. Bobrovsky, V. Shibaev, A. Bubnov, V. Hamplova, M. Kaspar, M. Glogarová, *Macromolecules* **2013**, *46*, 4276.
[10] P. Rizzo, C. Daniel, G. Guerra, *Macromolecules* **2010**, *43*, 1882.
[11] E. A. Mamonov, I. A. Kolmychek, S. Vandendriessche, M. Hojeij, Y. Ekinci, V. K. Valev, T. Verbiest, T. V. Murzina, *Phys. Rev. B* **2014**, *89*, 121113.
[12] E. Ozbay, *Science* **2006**, *311*, 189.
[13] M. Aeschlimann, M. Bauer, D. Bayer, T. Brixner, F. J. G. de Abajo, W. Pfeiffer, M. Rohmer, C. Spindler, F. Steeb, *Nature* **2007**, *446*, 301.
[14] I. Lieberman, G. Shemer, T. Fried, E. M. Kosower, G. Markovich, *Angew. Chem., Int. Ed.* **2008**, *47*, 4855.
[15] M. Schaferling, X. Yin, H. Giessen, *Opt. Express* **2012**, *20*, 26326.
[16] S. Yoo, Q.-H. Park, *Phys. Rev. Lett.* **2015**, *114*, 203003.
[17] D. Venkatakrishnarao, C. Sahoo, E. A. Mamonov, I. A. Kolmychek, A. I. Maydykovskiy, N. V. Mitetelo, V. B. Novikov, S. R. G. Naraharisetty, T. V. Murzina, R. Chandrasekar, *J. Mater. Chem. C* **2017**, *5*, 12349.
[18] N. Mitetelo, D. Venkatakrishnarao, J. Ravi, M. Popov, E. Mamonov, T. V. Murzina, R. Chandrasekar, *Adv. Opt. Mater.* **2019**, *7*, 1801775.
[19] Y. C. Tao, X. D. Wang, L. S. Liao, *J. Mater. Chem. C* **2019**, *7*, 3443.
[20] D. Venkatakrishnarao, E. A. Mamonov, T. V. Murzina, R. Chandrasekar, *Adv. Opt. Mater.* **2018**, *6*, 1800343.
[21] V. Radhika, D. Venkatakrishnarao, C. Sahoo, S. R. G. Naraharisetty, D. N. Rao, K. Müllen, R. Chandrasekar, *ACS Appl. Mater. Interfaces* **2018**, *10*, 16723.
[22] X. Wang, Q. Liao, Q. Kong, Y. Zhang, Z. Xu, X. Lu, H. Fu, *Angew. Chem., Int. Ed.* **2014**, *53*, 5863.
[23] X. Wang, Q. Liao, H. Li, S. Bai, Y. Wu, X. Lu, H. Hu, Q. Shi, H. Fu, *J. Am. Chem. Soc.* **2015**, *137*, 9289.
[24] D. Venkatakrishnarao, R. Chandrasekar, *Adv. Opt. Mater.* **2016**, *4*, 112.
[25] K. Tabata, D. Braam, S. Kushida, L. Tong, J. Kuwabara, T. Kanbara, A. Beckel, A. Lorke, Y. Yamamoto, *Sci. Rep.* **2015**, *4*, 5902.
[26] F. Panzer, M. Sommer, H. Bässler, M. Thelakkat, A. Köhler, *Macromolecules* **2015**, *48*, 1543.
[27] F. Panzer, H. Bässler, A. Köhler, *J. Phys. Chem. Lett.* **2017**, *8*, 114.
[28] F. C. Spano, C. Silva, *Annu. Rev. Phys. Chem.* **2014**, *65*, 477.
[29] D. Kim, J.-L. Brédas, *J. Am. Chem. Soc.* **2009**, *131*, 11371.
[30] D. A. Doval, S. Matile, *Org. Biomol. Chem.* **2013**, *11*, 7467.
[31] F. C. Spano, *Acc. Chem. Res.* **2010**, *43*, 429.
[32] A. Banerjee, A. A. Ogale, C. Das, K. Mitra, C. Subramanian, *Heat Transfer Eng.* **2005**, *26*, 41.
[33] K. Sugioka, M. Meunier, A. Piqué, *Laser Precision Microfabrication*, Springer Series in Materials Science, Vol. *135*, Springer-Verlag, Berlin Heidelberg **2010**.
[34] Y. S. L. V. Narayana, S. Basak, M. Baumgarten, K. Müllen, R. Chandrasekar, *Adv. Funct. Mater.* **2013**, *23*, 5875.
[35] C. Weder, M. S. Wrighton, *Macromolecules* **1996**, *29*, 5157.
[36] K. Hirose, K. Miura, Y. Senda, Y. Tobe, *Chem. Commun.* **2012**, *48*, 6052.

[37] R. Gatri, I. Ouerfelli, M. L. Efrit, F. S. Spirau, J.-P. Porte, P. Valvin, T. Roisnel, S. Bivaud, H. A. Kilig, J.-L. Fillaut, *Organometallics* **2014**, *33*, 665.

[38] H.-J. Deussen, E. Hendrickx, C. Boutton, D. Krog, K. Clays, K. Bechgaard, A. Persoons, T. Bjørnholm, *J. Am. Chem. Soc.* **1996**, *118*, 6841.

[39] N. Zhou, Y. Zhao, *J. Org. Chem.* **2010**, *75*, 1498.

[40] H. Zhang, X. Zheng, R. T. K. Kwok, J. Wang, N. L. C. Leung, L. Shi, J. Z. Sun, Z. Tang, J. W. Y. Lam, A. Qin, B. Z. Tang, *Nat. Commun.* **2018**, *9*, 4961.

[41] T. P. Martin, A. J. Wise, E. Busby, J. Gao, J. D. Roehling, M. J. Ford, D. S. Larsen, A. J. Moulé, J. K. Grey, *J. Phys. Chem. B* **2013**, *117*, 4478.

[42] M. E. Ziffer, S. B. Jo, Y. Liu, H. Zhong, J. C. Mohammed, J. S. Harrison, A. K.-Y. Jen, D. S. Ginger, *J. Phys. Chem. C* **2018**, *122*, 18860.